Biochemical and Biophysical Research Communications 447 (2014) 465–470

Contents lists available at ScienceDirect

Biochemical and Biophysical Research Communications

journal homepage: www.elsevier.com/locate/ybbrc

Significant decrease of ADP release rate underlies the potent activity of dimethylenastron to inhibit mitotic kinesin Eg5 and cancer cell proliferation ☆

Linlin Sun [a], Xiaodong Sun [c], Songbo Xie [c], Haiyang Yu [c,1], Diansheng Zhong [a,b,*]

[a] Lung Cancer Institute, Tianjin Medical University General Hospital, 154 Anshan Road, Heping District, Tianjin 300052, China
[b] Department of Oncology, Tianjin Medical University General Hospital, 154 Anshan Road, Heping District, Tianjin 300052, China
[c] Department of Genetics and Cell Biology, College of Life Sciences, Nankai University, 94 Weijin Road, Tianjin 300071, China

ARTICLE INFO

Article history:
Received 28 March 2014
Available online 13 April 2014

Keywords:
Eg5 inhibitor
Mitotic arrest
Apoptosis
ATPase activity
ADP release

ABSTRACT

Eg5 is a mitotic kinesin that plays a crucial role in the formation of bipolar mitotic spindles, by hydrolyzing ATP to push apart anti-parallel microtubules. Dimethylenastron is potent specific small molecule inhibitor of Eg5. The mechanism by which dimethylenastron inhibits Eg5 function remains unclear. By comparing with enastron, here we report that dimethylenastron prevents the growth of pancreatic and lung cancer cells more effectively, by halting mitotic progression and triggering apoptosis. We analyze their interactions with ADP-bound Eg5 crystal structure, and find that dimethylenastron binds Eg5 motor domain with higher affinity. In addition, dimethylenastron allosterically blocks the conformational change of the "sandwich"-like ADP-binding pocket more effectively. We subsequently use biochemical approach to reveal that dimethylenastron slows ADP release more significantly than enastron. These data thus provide biological, structural and mechanistic insights into the potent inhibitory activity of dimethylenastron.

1. Introduction

Anticancer drugs that interfere with mitosis, such as taxanes and vinca alkaloids, have been widely used in the clinical therapy of human malignancies [1,2]. They target tubulin, a key protein component of the mitotic spindle. However, clinical use of these microtubule inhibitors often leads to dose-limiting toxicities, because microtubules are also involved in many other cellular processes, such as cell motility, maintenance of cell shape, and intracellular transport [3].

The kinesin family of motor proteins is emerging as an attractive target for specific anti-mitotic cancer therapies [4]. These kinesins are abundant in hyper-proliferative cells, i.e. cancer cells, and barely expressed in non-dividing cells [5]. As a member of the kinesin family, Eg5 (also known as kinesin-5 or kinesin spindle protein, KSP) plays essential roles in bipolar spindle assembly, by hydrolyzing ATP to push apart anti-parallel microtubules and separate the duplicated centrosomes [6–8]. Similar to other kinesins, Eg5 contains a motor domain, which mediates interactions with microtubule and ATP hydrolysis.

Specific small molecule inhibitors of Eg5 represent a new generation of chemotherapeutic compounds [9–11], some of which have been examined in phase I and II clinical trials [12,13]. Dimethylenastron, the dihydropyrimidine (DHPM)-derived analog, is developed as a potent inhibitor of Eg5 by Gartner et al. [14] in an initial SAR study. However, its biologic effects and mechanism of action are not well understood. In this study, by comparing with the analog enastron, we sought to determine the molecular basis for the potent Eg5 inhibition by dimethylenastron.

2. Materials and methods

2.1. Materials

Dimethylenastron and enastron were provided by Drs. Vasiliki Sarli and Athanassios Giannis (University of Leipzig, Germany).

☆ This work was supported by grants from the National Natural Science Foundation of China (81071915 and 31301160) and Tianjin Municipal Health Bureau (2011KZ107). The funders had no role in study design, data collection and analysis, decision to publish, or preparation of the manuscript.

* Corresponding author at: Department of Oncology, Tianjin Medical University General Hospital, 154 Anshan Road, Heping District, Tianjin 300052, China. Fax: +86 22 60363013.
E-mail address: Zhongdsh@hotmail.com (D. Zhong).
[1] Present address: Department of Pathology and Immunology, Washington University in St. Louis, MO, USA.

http://dx.doi.org/10.1016/j.bbrc.2014.04.023
0006-291X/

Sulforhodamine B (SRB), 4′-6-diamidino-2-phenylindole (DAPI) and propidium iodide (PI) were purchased from Sigma–Aldrich (St. Louis, MO, US). The Rabbit antibody against PARP was from Cell Signaling Technology (Beverly, MA, US) and the mouse monoantibody against GAPDH was from Santa Cruz Biotechnology (Santa Cruz, CA, US).

2.2. Cell culture

EPP85 human pancreatic cancer cells, PC9 and A549 human lung cancer cells (ATCC) were cultured in RPMI 1640 medium (Gibico, USA) supplemented with 10% fetal bovine serum (Gibico, USA) at 37 °C in a humidified atmosphere with 5% CO_2.

2.3. In vitro cell proliferation assay

Cells grown in 96-well culture plates were treated with gradient concentrations of dimethylenastron or enastron for 48 h and were fixed with 10% trichloroacetic acid and stained with 0.4% SRB dissolved in 1% acetic acid. The cells were then washed with 1% acetic acid to remove unbound dye. The protein-bound dye was extracted with 10 mM Tris base to determine the optical density at 490 nm wavelength. The percentage of cell proliferation as a function of drug concentration was plotted to determine IC50, which stands for the drug concentration needed for 50% inhibition of cell proliferation.

2.4. Fluorescence microscopy

Cells grown on glass coverslips were fixed with cold (−20 °C) methanol for 5 min and then washed with phosphate-buffered saline (PBS), followed by staining with DAPI for 5 min. Coverslips were then mounted with 90% glycerol in PBS and examined with an Olympus fluorescence microscope.

2.5. Flow cytometry

$2 * 10^6$ cells were collected, washed twice with ice-cold PBS, and fixed in 70% ethanol for 24 h. Cells were washed again with PBS and incubated with PI (20 μg/ml) and RNaseA (20 μg/ml) in PBS for 30 min in the dark. Samples were analyzed on a BD FACSCalibur flow cytometer.

2.6. Western blot analysis

Proteins were resolved by polyacrylamide gel electrophoresis and transferred onto polyvinylidene difluoride (PVDF) membranes (Millipore, Germany). The membranes were blocked in Tris-buffered saline containing 0.2% Tween 20 and 5% fat-free dry milk and incubated first with primary antibodies and then with horseradish peroxidase-conjugated secondary antibodies. Specific proteins were visualized with enhanced chemiluminescence detection reagent according to the manufacturer's instructions (Pierce Biotechnology, USA).

2.7. Structural analysis

The coordinates of ADP–Eg5 structure (PDB: 1II6), ADP–Eg5–dimethylenastron structure (PDB: 2X7D) and ADP–Eg5–enastron structure (PDB: 2X7C) were obtained from the Protein Data Base [15,16] and subsequently analyzed.

2.8. Measurement of Eg5 ATPase activity

The ATPase activity of Eg5 was examined with the pyruvate kinase–lactate dehydrogenase detection system as described previously [5]. Changes in optical density were measured at a wavelength of 340 nm using a microplate reader (Molecular Devices, USA). The percentage of ATPase activity as a function of drug concentration was plotted to determine IC50, which stands for the drug concentration needed for 50% inhibition of ATPase activity.

2.9. Analysis of ADP release rate

The ADP release rate of Eg5 motor domain was examined with the MANT-ADP reagent (Molecular Probes), by measuring the changes in MANT-ADP fluorescence as described previously [5,17]. Briefly, purified Eg5 motor domain was incubated with the MANT-ADP racemate at a 1:1 stoichiometry. The Eg5–MANT-ADP complex was then mixed with 1 mmol/L MgATP in the absence of microtubules. The decrease in MANT-ADP fluorescence was examined over time at an excitation wavelength of 360 nm and an emission wavelength of 460 nm. The observed exponential rate constant was subsequently fit to a hyperbola to obtain the ADP release rate.

2.10. Statistical analysis

Experiments were repeated 3 times, and error bars represent standard deviations between experiments.

3. Results

3.1. Dimethylenastron displays higher anti-proliferative activity than enastron

To investigate the effects of dimethylenastron or enastron on the growth of pancreatic cancer cells, EPP85 human pancreatic cancer cells were treated with gradient concentrations of the two compounds respectively. Cell proliferation was measured by sulforhodamine B staining assay [18]and the IC50 values were then determined. As shown in Fig. 1A, dimethylenastron (DIMEN), with an IC50 of 0.37 μM, was about 10 times more potent than enastron (IC50 = 4.57 μM) in inhibiting the growth of EPP85 cells. To directly investigate the anti-proliferative activity of the two chemicals in lung cancer cells, we used phase contrast microscopic analysis to examine the cell morphology after 48 h drug treatment. We found that most of the PC9 lung cancer cells turned round and appeared fragmented in the presence of 1 μM dimethylenastron, whereas they proliferated normally upon 1 μM enastron treatment (Fig. 1B). Thus, dimethylenastron inhibits the growth of cancer cells more potently than enastron.

3.2. Dimethylenastron halts mitotic progression and triggers apoptosis more significantly than enastron

To test whether the dimethylenastron-induced growth inhibition was mediated by mitotic arrest, we examined cellular DNA in the drug-treated EPP85 cells with the DNA dye (DAPI) by fluorescence microscopy. As shown in Fig. 2A, 24-h dimethylenastron treatment led to a higher percentage (32.43%) of EPP85 cells with condensed chromosomes, while enastron exposure resulted in fewer cells blocked at mitosis (7.40%). Similar result was achieved by flow cytometric analysis of cellular DNA content in A549 lung cancer cells. As shown in Fig. 2B, 1 μM dimethylenastron promoted a significant increase in the number of G2/M phase cells with duplicated DNA content. In contrast, 1 μM enastron induced no obvious changes of cell cycle distribution. We used a higher concentration (5 μM) of enastron to achieve the similar effect of 1 μM dimethylenastron treatment. Therefore, these results show

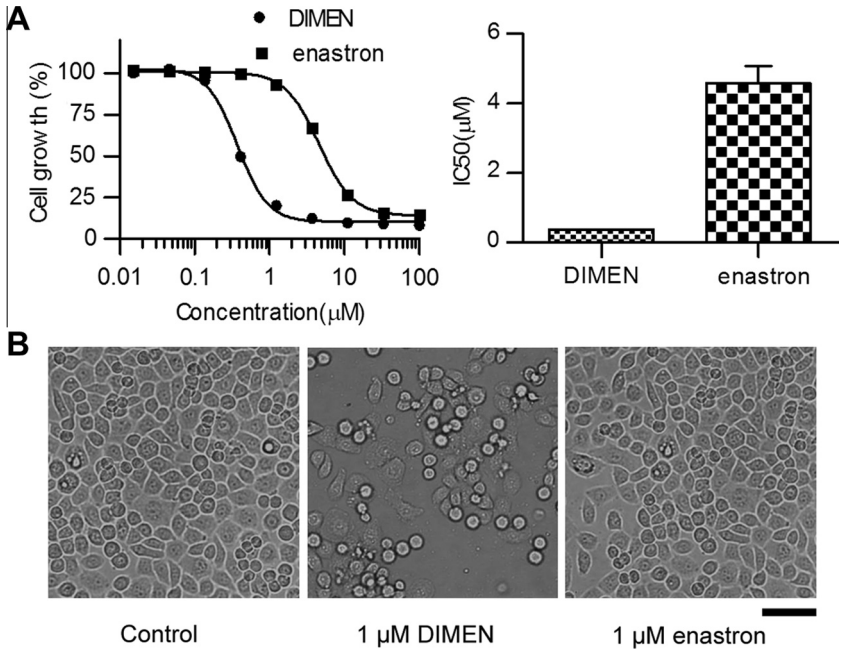

Fig. 1. Dimethylenastron displays higher anti-proliferative activity than enastron. (A) EPP85 pancreatic cancer cells were treated with varying concentrations of dimethylenastron or enastron for 48 h, and IC50 values were then determined by sulforhodamine B-based in vitro cell proliferation assay. (B) Phase contrast images of PC9 lung cancer cells treated with 1 μM dimethylenastron or enastron for 48 h. Size bar, 50 μm.

that dimethylenastron halts mitotic progression more dramatically than enastron.

The morphology of fragmented cells upon prolonged dimethylenastron treatment (Fig. 1B) indicated the induction of cell apoptosis by the drug. We subsequently examined the nuclear morphology of EPP85 cells by staining the drug-treated cells with DAPI to further investigate the incidence of apoptosis. As shown in Fig. 2C, 48-h treatment with 1 μM dimethylenastron induced the formation of condensed and fragmented nuclei (known as apoptotic bodies) characteristic of apoptosis, while few apoptotic cells were observed upon enastron treatment. To validate our observation, the cleavage of poly (ADP-ribose) polymerase (PARP), an apoptotic marker, was examined in the drug-treated A549 cells. Compared with enastron, dimethylenastron led to the cleavage of PARP more significantly (Fig. 2D). Collectively, these results demonstrate that dimethylenastron triggers apoptosis more robustly than enastron in cancer cells.

3.3. Dimethylenastron allosterically blocked the conformational change of the ADP-binding pocket more effectively than enastron

To achieve mechanistic insight into the increased potency of dimethylenastron in suppressing cell growth, we analyzed its interactions with ADP-bound Eg5 crystal structure [15,16]. As shown in Fig. 3A, the helix α2 is interrupted by a flexible loop referred as L5. The dimethylenastron-binding pocket is bordered by helix α2, loop L5 and helix α3. This binding site is in close proximity to the ADP-binding pocket in Eg5 motor domain. As Fig. 3B shows, the adenine-binding pocket is a hydrophobic "sandwich"-like structure. A detailed analysis in Fig. 3C revealed that the adenine ring is bound in a hydrophobic groove, like a "patty" placed inside a "sandwich". The propyl-group of Arg26 and the ring of Pro27 from sheet b1 join together to form the upper "bun" of the "sandwich", while the phenyl-group of Phe113 on helix α2 serves as the lower "bun". The Phe113 resides close to the aforementioned loop L5, which is motile to modulate the conformational change of the "sandwich" needed for ADP release [19,20].

When dimethylenastron or enastron binds to the interface between helixes α2 and α3, the loop L5 is no longer motile; thus the inhibitor appears to act as a "latch" connecting helixes α2 and α3, providing steric blockage of the L5 (Fig. 3D). Detailed analysis of the ADP–Eg5 structure bound with the two drugs are shown separately in Fig. 3E. Their interactions with the residues of the binding site were largely identical. They both have a phenyl group, which forms hydrogen bond with the peptide bond of Leu132–Ala133 on helix α2. The other side of the compound forms hydrophobic interaction with the residues on helix α3 (Tyr211 and Ala218). Dimethylenastron shows much higher affinity to the binding site than enastron, because the di-methyl group maintains stronger hydrophobic interactions with Tyr211 and Ala218. Without the dimethyl modification, enastron weakly interacts with the helix α3. Taken together, we proposed a model that dimethylenastron, with higher affinity to Eg5, latches the loop L5 more tightly, thereby inducing conformational rigidity and trapping ADP into the "sandwich"-like ADP-binding pocket more potently than enastron .

3.4. Dimethylenastron slows ADP release and inhibits Eg5 ATPase activity more potently than enastron

The analysis of crystal structures indicated that dimethylenastron inhibits Eg5 ATPase activity more potently than enastron. To test this hypothesis, an in vitro steady-state ATPase assay was used. As shown in Fig. 4A, both of the two compounds abolished Eg5 ATPase activity. Dimethylenastron (IC50 = 0.24 μM) showed 10 times higher potency in inhibiting Eg5 ATPase activity than enastron (IC50 = 2.49 μM). To investigate whether dimethylenastron inhibits Eg5 activity by affecting ADP release, we monitored the ADP release rate of Eg5 motor domain by the use of MANT-ADP [5], a fluorescent analog of ADP that displays increased fluorescence when bound to Eg5 [17]. As shown in Fig. 4B, dimethylenastron induced a 70-fold reduction in the basal rate of ADP release (in the absence of microtubules), while enastron only led to a 5-fold reduction. These data thus suggest that the potent inhibition of dimethylenastron on Eg5 ATPase activity is, at least

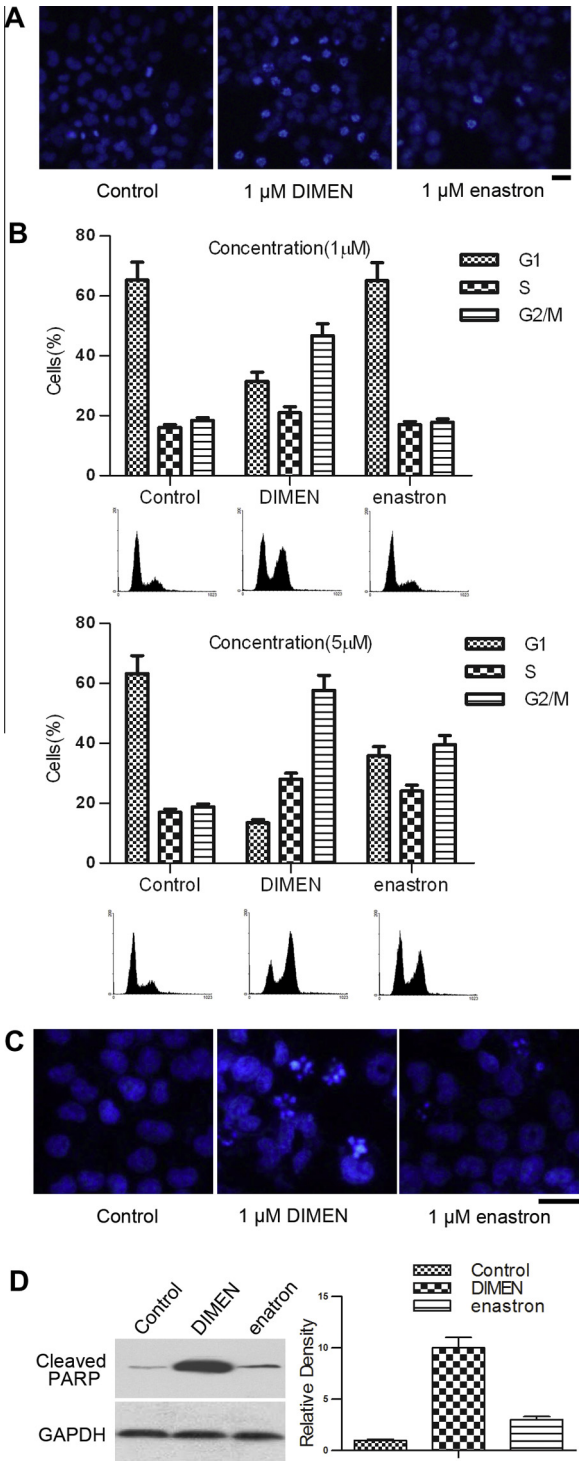

Fig. 2. Dimethylenastron halts mitotic progression and triggers apoptosis more significantly than enastron. (A) EPP85 cells were treated with 1 μM dimethylenastron or enastron for 24 h, stained with the DNA dye DAPI and then observed under a fluorescence microscope. Size bar, 10 μm. (B) Flow cytometric analysis of A549 lung cancer cells treated with dimethylenastron or enastron (1 μM or 5 μM) for 24 h. The amplitude of curves corresponds to the cell number. The peak on the left represents cells in G1 phase of cell cycle, while the right peak represents cells in G2/M phase. (C) Fluorescence images of DAPI-stained nuclei in EPP85 cells treated with 1 μM dimethylenastron or enastron for 48 h. Size bar, 10 μm. (D) A549 cells were treated with 1 μM dimethylenastron or enastron for 48 h and cellular cleaved PARP was analyzed using Western blot.

partially, due to its ability to slow ADP release more dramatically than enastron, independent of the microtubule binding.

4. Discussion

Dimethylenastron and its analog enastron have been identified as specific Eg5 inhibitors by Gartner et al. [14]. In the present study, we performed a series of experiments to gain a more thorough understanding of the biologic effects by the two drugs. We found that dimethylenastron inhibited cell growth more potently than enastron, by arresting cell-cycle progression at mitosis and inducing apoptosis in pancreatic and lung cancer cells. The findings further indicate dimethylenastron as a more effective anticancer drug.

While the crystal structure of ADP-bound Eg5 have been solved by Turner et al. [15], the interactions between ADP and Eg5 have never been analyzed in detail. In this study, we reported a hydrophobic "sandwich"-like structure of the adenine-binding pocket. The hydrophobic side chains lining the binding pocket act as the two "buns" of a "sandwich", while the adenine is the "patty" inside the "sandwich". The conformational change of the "sandwich", which is required for ADP release, is expected to be regulated by the motile loop L5 [19,20]. Interestingly, the hydrophobic "sandwich"-like structure is a characteristic structure frequently seen in the protein kinase, termed "hydrophobic core" [21,22]. Without this core, ATP cannot be hydrolyzed because the structure is not stable. Hence, this proposed "sandwich" model will not only aid in better understanding how ADP is released from Eg5, but also suggest the intriguing possibility that the hydrophobic core is a common feature for all the ATPases, including kinases and motor proteins. Additional biochemical experiments are needed to verify the model in future studies. It is predicted that mutation of the aforementioned residue (F113A) lining the hydrophobic core may lead to decreased ATPase activity.

According to the crystal structure of Eg5 bound with dimethylenastron or enastron reported by Kaan et al. [16], dimethylenastron is better fit to the allosteric binding site than enastron. In good agreement with their analysis, we also found that the two additional methyl groups on dimethylenastron maintain stronger hydrophobic interactions with Tyr211 and Ala218 on helix α3 than enastron. Moreover, we herein proposed a "latch" model that the inhibitors serve as a "latch" connecting the helix α2 and α3 and locking the loop L5, which may explain why higher affinity of dimethylenastron to Eg5 motor domain leads to the increased potency. Since the loop L5 is the target for a number of allosteric Eg5 inhibitors [23,24], it is likely that our proposed "latch" model provides a common mechanism of action for these small molecule inhibitors. With these inhibitors binding to the pocket outside the loop L5, L5 is not flexible; thus the aforementioned "sandwich" is locked and ADP is trapped into the hydrophobic core.

The Eg5 motor domain undergoes a complex kinetic cycle of ATP binding, ATP hydrolysis and sequential ADP release [5]. Inhibition of Eg5 ATPase activity could result from competing with ATP binding or allosteric disruption [25]. On the structural basis of ADP-bound Eg5 in complex with the drugs, we hypothesized that dimethylenastron allosterically trapped ADP into its binding pocket more effectively than enastron. This model prompted us to compare their effects on ADP release. As expected, we found that dimethylenastron inhibited the basal rate of ADP release rate more efficiently than enastron, verifying our hypothesis derived from structural analysis. Therefore, we concluded that the potent inhibition of Eg5 ATPase activity by dimethylenastron is largely attributable to the significant blockage of ADP release. In addition, the dimethylenastron inhibition of ADP release is independent of the Eg5/microtubule interaction, suggesting that dimethylenastron would might not affect the normal physiologic functions of Eg5 that require its interaction with microtubules and serves as a good chemotherapeutic agent that might have few side effects.

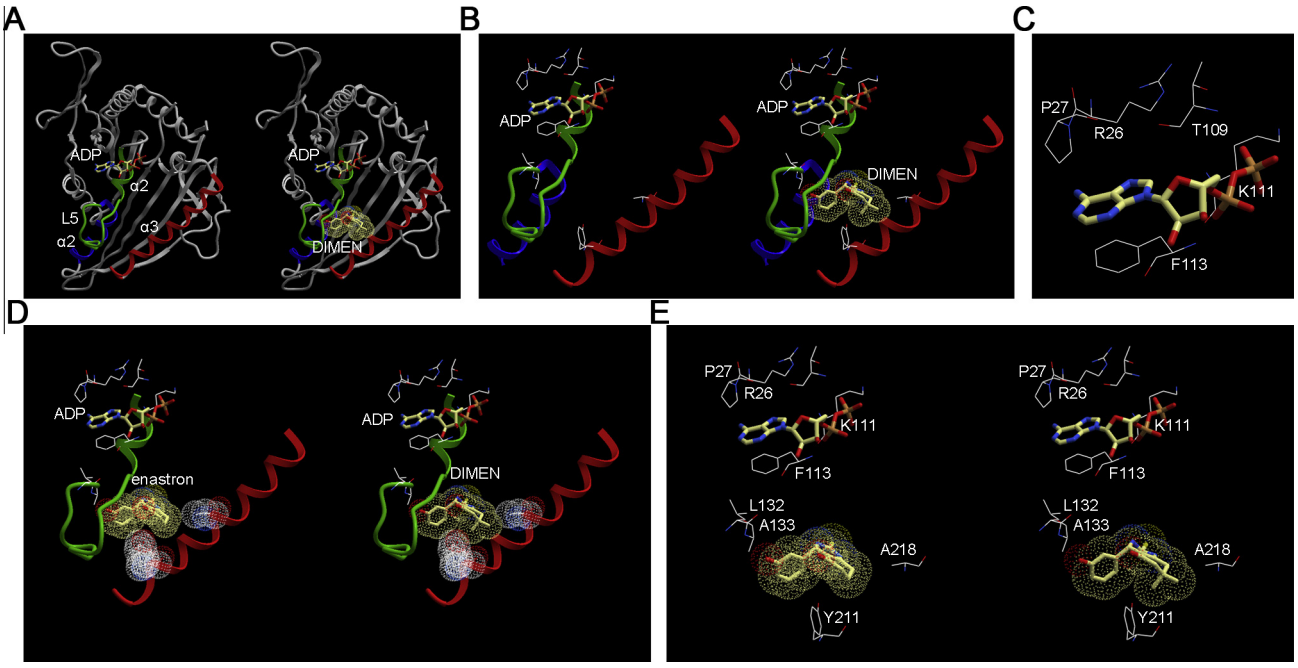

Fig. 3. Dimethylenastron allosterically blocked the conformational change of the ADP-binding pocket more effectively than enastron. (A) A stereo ribbon representation of ADP-bound Eg5 crystal structure with (right) or without dimethylenastron (left). Helix α2 is shown in green and blue, and helix α3 is shown in red. ADP (upper) and dimethylenastron (lower) are represented in the stereo view by color-coded sticks. (B) An enlarged stereo ribbon representation of ADP-bound Eg5 crystal structure with (right) or without dimethylenastron (left). The side chains lining the ADP-binding site (upper) and drug-binding pocket (lower) are shown. (C) Important amino acid residues involved in the ADP–Eg5 interactions. Arg26, Pro27 and Phe113 are labeled to depict their locations. (D) An enlarged stereo ribbon representation of ADP-bound Eg5 crystal structure in the presence of dimethylenastron (right) or enastron (left). The side chains lining the ADP-binding site (upper) and drug-binding pocket (lower) are shown. (E) Important amino acid residues involved in the interactions with dimethylenastron (right) or enastron (left). Leu132, Ala133, Tyr211 and Ala218 are labeled to depict their locations. (For interpretation of the references to color in this figure legend, the reader is referred to the web version of this article.)

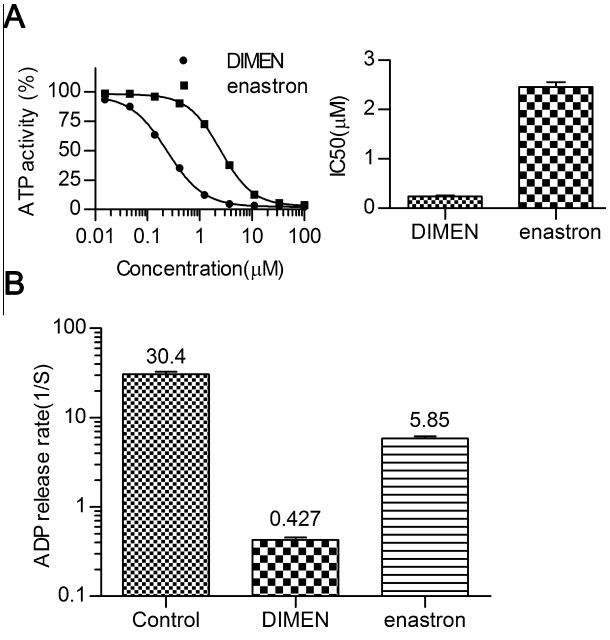

Fig. 4. Dimethylenastron slows ADP release and inhibits Eg5 ATPase activity more potently than enastron. (A) Effects of dimethylenastron or enastron on Eg5 ATPase activity were examined with in vitro steady-state ATPase assay and IC50 values were then determined. (B) The effect of dimethylenastron or enastron on ADP release rate of the Eg5 motor domain in the absence of microtubules was examined by measuring the changes in MANT-ADP fluorescence.

In conclusion, by comparison with enastron, our results further demonstrate the potent anti-proliferation activity of dimethylenastron and reveal its mechanism of action. Firstly, we reported that dimethylenastron-induced growth inhibition of cancer cells was mediated by dramatic mitotic arrest and profound apoptosis, achieving a more thorough biologic evaluation of the drug. Secondly, based on structural analysis of ADP–Eg5 bound with the drugs, we proposed a "sandwich" and "latch" model that dimethylenastron "latches" the loop L5 more tightly and allosterically blocks the conformational change of the "sandwich"-like ADP-binding pocket more effectively than enastron, providing a good explanation for how structural differences between the two drugs contribute to their varying levels of potency. Finally, by biochemical approach we confirmed that dimethylenastron hindered ADP release more significantly than enastron, thus shedding mechanistic lights on the increased potency of dimethylenastron. Our study may provide novel insights into the design of structure-based anticancer drugs.

Acknowledgments

We would like to thank Drs. Vasiliki Sarli and Athanassios Giannis (University of Leipzig, Germany) for providing reagents. We also thank Drs. Jun Zhou (Nankai University, China) and Min Liu (Tianjin Medical University, China) for discussions and suggestions on the project.

References

[1] K.W. Wood, W.D. Cornwell, J.R. Jackson, Past and future of the mitotic spindle as an oncology target, Curr. Opin. Pharmacol. 1 (2001) 370–377.
[2] M.A. Jordan, L. Wilson, Microtubules as a target for anticancer drugs, Nat. Rev. Cancer 4 (2004) 253–265.
[3] H.C. Joshi, Microtubule dynamics in living cells, Curr. Opin. Cell Biol. 10 (1998) 35–44.
[4] O. Rath, F. Kozielski, Kinesins and cancer, Nat. Rev. Cancer 12 (2012) 527–539.
[5] R. Sakowicz, J.T. Finer, C. Beraud, A. Crompton, E. Lewis, A. Fritsch, Y. Lee, J. Mak, R. Moody, R. Turincio, J.C. Chabala, P. Gonzales, S. Roth, S. Weitman, K.W. Wood, Antitumor activity of a kinesin inhibitor, Cancer Res. 64 (2004) 3276–3280.

[6] M.T. Valentine, S.P. Gilbert, To step or not to step? How biochemistry and mechanics influence processivity in Kinesin and Eg5, Curr. Opin. Cell Biol. 19 (2007) 75–81.
[7] A.S. Kashina, G.C. Rogers, J.M. Scholey, The bimC family of kinesins: essential bipolar mitotic motors driving centrosome separation, Biochim. Biophys. Acta 1357 (1997) 257–271.
[8] L.C. Kapitein, E.J. Peterman, B.H. Kwok, J.H. Kim, T.M. Kapoor, C.F. Schmidt, The bipolar mitotic kinesin Eg5 moves on both microtubules that it crosslinks, Nature 435 (2005) 114–118.
[9] T.U. Mayer, T.M. Kapoor, S.J. Haggarty, R.W. King, S.L. Schreiber, T.J. Mitchison, Small molecule inhibitor of mitotic spindle bipolarity identified in a phenotype-based screen, Science 286 (1999) 971–974.
[10] T.M. Kapoor, T.U. Mayer, M.L. Coughlin, T.J. Mitchison, Probing spindle assembly mechanisms with monastrol, a small molecule inhibitor of the mitotic kinesin, Eg5, J. Cell Biol. 150 (2000) 975–988.
[11] S. Hotha, J.C. Yarrow, J.G. Yang, S. Garrett, K.V. Renduchintala, T.U. Mayer, T.M. Kapoor, HR22C16: a potent small-molecule probe for the dynamics of cell division, Angew. Chem. Int. Ed. Engl. 42 (2003) 2379–2382.
[12] D.M. Duhl, P.A. Renhowe, Inhibitors of kinesin motor proteins – research and clinical progress, Curr. Opin. Drug Discov. Devel. 8 (2005) 431–436.
[13] H.B. El-Nassan, Advances in the discovery of kinesin spindle protein (Eg5) inhibitors as antitumor agents, Eur. J. Med. Chem. 62 (2013) 614–631.
[14] M. Gartner, N. Sunder-Plassmann, J. Seiler, M. Utz, I. Vernos, T. Surrey, A. Giannis, Development and biological evaluation of potent and specific inhibitors of mitotic kinesin Eg5, ChemBioChem 6 (2005) 1173–1177.
[15] J. Turner, R. Anderson, J. Guo, C. Beraud, R. Fletterick, R. Sakowicz, Crystal structure of the mitotic spindle kinesin Eg5 reveals a novel conformation of the neck-linker, J. Biol. Chem. 276 (2001) 25496–25502.
[16] H.Y. Kaan, V. Ulaganathan, O. Rath, H. Prokopcova, D. Dallinger, C.O. Kappe, F. Kozielski, Structural basis for inhibition of Eg5 by dihydropyrimidines: stereoselectivity of antimitotic inhibitors enastron, dimethylenastron and fluorastrol, J. Med. Chem. 53 (2010) 5676–5683.
[17] S.P. Gilbert, A.T. Mackey, Kinetics: a tool to study molecular motors, Methods 22 (2000) 337–354.
[18] V. Vichai, K. Kirtikara, Sulforhodamine B colorimetric assay for cytotoxicity screening, Nat. Protoc. 1 (2006) 1112–1116.
[19] J.S. Waitzman, A.G. Larson, J.C. Cochran, N. Naber, R. Cooke, F. Jon Kull, E. Pate, S.E. Rice, The loop 5 element structurally and kinetically coordinates dimers of the human kinesin-5, Eg5, Biophys. J. 101 (2011) 2760–2769.
[20] J.M. Muretta, W.M. Behnke-Parks, J. Major, K.J. Petersen, A. Goulet, C.A. Moores, D.D. Thomas, S.S. Rosenfeld, Loop L5 assumes three distinct orientations during the ATPase cycle of the mitotic kinesin Eg5: a transient and time-resolved fluorescence study, J. Biol. Chem. 288 (2013) 34839–34849.
[21] A.P. Kornev, N.M. Haste, S.S. Taylor, L.F. Eyck, Surface comparison of active and inactive protein kinases identifies a conserved activation mechanism, Proc. Natl. Acad. Sci. U.S.A. 103 (2006) 17783–17788.
[22] A.P. Kornev, S.S. Taylor, L.F. Ten Eyck, A helix scaffold for the assembly of active protein kinases, Proc. Natl. Acad. Sci. U.S.A. 105 (2008) 14377–14382.
[23] Y. Yan, V. Sardana, B. Xu, C. Homnick, W. Halczenko, C.A. Buser, M. Schaber, G.D. Hartman, H.E. Huber, L.C. Kuo, Inhibition of a mitotic motor protein: where, how, and conformational consequences, J. Mol. Biol. 335 (2004) 547–554.
[24] L. Lad, L. Luo, J.D. Carson, K.W. Wood, J.J. Hartman, R.A. Copeland, R. Sakowicz, Mechanism of inhibition of human KSP by ispinesib, Biochemistry 47 (2008) 3576–3585.
[25] Z. Maliga, T.M. Kapoor, T.J. Mitchison, Evidence that monastrol is an allosteric inhibitor of the mitotic kinesin Eg5, Chem. Biol. 9 (2002) 989–996.